Macromolecules

ARTICLE

pubs.acs.org/Macromolecules

Synthesis and Characterization of Fluorescent Polymer−Metal Nanocomposites Comprising Poly(silylene-*co*-silyne)s and Silver Nanoparticles

Ravi Shankar,* Usharani Sahoo, and Vandana Shahi

Department of Chemistry, Indian Institute of Technology, Hauz Khas, New Delhi 110016, India

Supporting Information

ABSTRACT: Branched organosilicon polymers of composition $[(PhMeSi)_x\text{-}co\text{-}(RSi)_{1-x}]_n$ [x = 0.83−0.75, R = $Et_3SiCH_2CH_2$ (**1**), 2-$FuMe_2SiCH_2CH_2$ (Fu = Furyl, **2**), *n*-Hex (**3**), Ph (**4**)] have been synthesized by reacting a mixture of dichloromethylphenylsilane and an appropriate trichloroorganosilane, $RSiCl_3$ in 5:1 molar ratio with sodium dispersion in refluxing toluene (Wurtz coupling). A change in the feed ratio of $Et_3SiCH_2CH_2SiCl_3$ and $PhMeSiCl_2$ monomers to 1:1 affords the polymer, $[(PhMeSi)_{0.55}\text{-}co\text{-}(Et_3SiCH_2CH_2Si)_{0.45}]_n$, **5**, with increased domains of branching sites while the synthesis of polysilyne $[Et_3SiCH_2CH_2Si]_n$, **6**, involves the corresponding organotrichlorosilane as the precursor. The polysilanes, **1**−**4** act as excellent precursors for the reduction of silver acetate [polymer repeat unit: Ag^+ = 0.10, 0.25] under mild conditions (toluene, room temperature) and afford the formation of polymer−metal nanocomposites, **1a**−**4a** and **1b**−**4b** containing silver nanoparticles with an average diameter of 5−7 and 8−11 nm, respectively. The optical properties and fluorescent nature of these composites as green light emitters have been studied by UV−vis and photoluminescence (PL) spectroscopy as well as confocal microscopy. The results accord the formation of silver nanoclusters in conjunction with nanoparticles. The host polymer matrix devoid of silver nanoparticles is obtained in each case by addition of a donor solvent (THF) in the composites and subsequently characterized by GPC, PL and cyclic voltammetric studies. A substantial decrease in molecular weight (M_w = 4.8−10.4 × 10^3) with respect to that of the corresponding parent polysilane (M_w = 9.7−21.0 x10^3) suggests irreversible oxidative cleavage of the skeletal backbone. The results also provide a basis to conclude that reducing action of **1**−**4** toward Ag(I) ions is predominantly located in the polysilyne segments leading to partial inclusion of Si−O−Si bonds in the host polymer structures. The role of polymer composition on the optical properties of silver nanoparticles has been examined by studying the nanocomposites **5a** and **6a** derived from the polymers, **5** and **6** respectively. The results suggest that branched polysilanes, **1**−**5** are unique in acting as scaffolds for fluorescent silver nanoclusters.

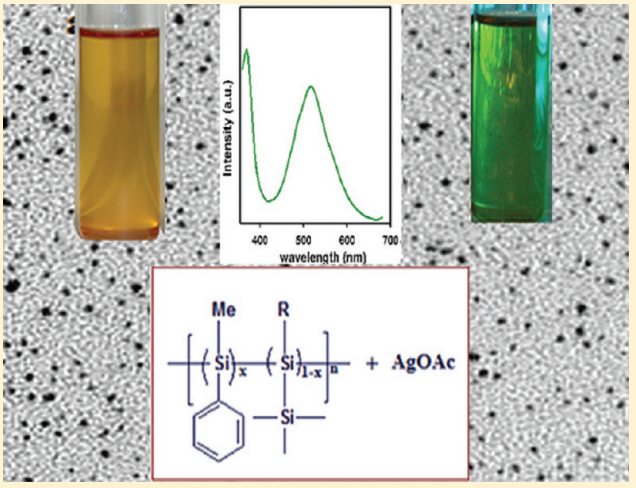

1. INTRODUCTION

Extensive studies on the electronic attributes of linear, high molecular weight polysilanes, $[R_2Si]_n$ (R = alkyl or aryl) in the past[1,2] have provided a great deal of thrust to explore potential applications of these polymers in the field of optoelectronics, semiconducting materials as well as ceramics. By virtue of σ-electron delocalized silicon backbone as well as amenable band gap energy (3−4 eV) associated with the framework structure, linear polysilanes have also been examined for their reducing behavior toward noble metal ions such as Ag(I), Au(III), Pd(II), and Pt(II) etc. Fukushima et al. have reported tentative assignment of the redox potential (+0.34 to +0.54 V) of linear poly(methylphenylsilane)s with respect to standard hydrogen electrode, suggesting their affinity to reduce metal ions with higher oxidation potential.[3] The approach has been successfully utilized for the synthesis of silicon based polymer−metal nanocomposites which exhibit excellent catalytic properties in many organic transformations.[4−9] Metal nanoparticles in polysilane/siloxane based matrices are considered to exhibit superior activity and selectivity toward catalytic reactions than bound to strong co-ordinating ligands due to weaker interactions between nanoparticles and polymer surfaces.[10−12] Notable among these are hydrogenation, Suzuki, Sonagashira coupling and hydrosilylation reactions. A recent report from our group has shown that poly(alkyl−arylsilane)s, $[R(C_6H_4\text{−}R^1)Si]_n$ (R = $Et_3SiCH_2CH_2$; R^1 = H, *p*-Me, *p*-OMe, *p*-NMe_2) exhibit variations in HOMO−LUMO

Received: January 10, 2011
Revised: March 25, 2011
Published: April 11, 2011

band gap energies as well as oxidation potentials (0.95−0.49 V) as a function of electron withdrawing/releasing substituents (R^1) on the phenyl group. This intrinsic property has been utilized to achieve control over size domains of *in situ* generated silver and palladium nanoparticles.[13] In addition, we have also demonstrated that the use of functional polysilanes bearing thienyl or furyl donor groups on the appended sila−alkyl side chains is advantageous to afford polymer−metal composites containing silver and palladium nanoparticles with long shelf life stability.[14,15] The passive behavior of these nanoparticles toward agglomeration in the functional polymer matrix originates from donor−acceptor interaction between thienyl/furyl group and the nanometal surface.

Polymer−metal nanocomposites incorporating small silver clusters such as Ag_2, Ag_3, and Ag_4, etc. have received considerable attention in view of their unique emissive properties in the visible region.[16−20] Recent studies have shown that, in contrast to nanoparticles, photoemission from silver nanoclusters originates from spatial confinement of free electrons and size-dependent discrete energy levels.[12,21] As a result, potential applications of the materials containing noble-metal nanoclusters/nanodots are being sought in single molecular spectroscopy, biological labeling, optical sensing, catalysis, etc.[22,23] Synthetic methods of these composites primarily rely on the use of external reducing agents and organic based functional dendrimers/multi arm star copolymers and biomolecules as templates which have the desirable properties to stabilize or encapsulate metal nanoclusters.[24−30]

Despite these developments, potential applications of higher dimensional silicon catenates such as polysilynes,[31−37] $[RSi]_n$ as well as poly(silylene-*co*-silyne)s,[38,39] $[(R_2Si)_x\text{-}co\text{-}(RSi)_{1\text{-}x}]_n$ (also known as network and branched polysilanes respectively) in the synthetic domain of noble metal nanoparticles/clusters have not been explored so far. A detailed understanding of this aspect is desired in view of available information on the electronic properties of these polymers which differ appreciably from those of linear polysilanes. Polysilynes are generally considered as soluble models of amorphous silicon and best represented as two-dimensional sheet-like structures comprising of linear, branched and cyclic components. These are associated with both direct and indirect band gaps of the order of 2−3 eV which are nearly degenerate and electronic properties can be tailored through surface chemical derivatization.[40] Krempner et al. have recently reported optical properties of oligosilane dendrimers and their analogous derivatives which possess oxo, hydroxo, or alkoxide groups.[41] These discrete molecular entities are considered as models for higher dimensional silicon catenates such as polysilynes and siloxenes. A significant aspect of these studies as well as those reported by others,[42,43] is the revelation that introduction of oxygen functionalities on catenated silicon frameworks significantly enhances room temperature photoluminescence properties in the visible region. On the basis of controlled vacuum pyrolysis studies of a number of polysilynes, Fujuki et al. have demonstrated that the materials derived there from exhibit wide range of visible light (blue to red) emissions at 77 K as a result of structural transformation which resembles that of Siloxene-like, multilayered sheet structure.[35] Relevant studies on the optical properties of branched polysilanes by UV−vis and PL (emission) spectroscopy as well as fluorescence lifetime decay measurements have shown that linear and branched units of these polymers more or less behave as separate chromophores and exhibit distinct photophysical properties.[38,39] On the basis of these studies, it is suggested that the extent of σ-delocalization in the skeletal backbone increases with higher degree of branching sites in the structural framework.

As part of our continued interest in polysilane chemistry,[13−15] we endeavored to explore fundamental issues concerning the role of branched polysilanes as reducing agents for Ag(I) ions as well as their affinity to function as the scaffolds for *in situ* generated metal nanoparticles. As a prerequisite, branched polysilanes, $[(PhMeSi)_x\text{-}co\text{-}(RSi)_{1\text{-}x}]_n$ [x = 0.83−0.75, R = $Et_3SiCH_2CH_2Si$ (**1**), 2-$FuMe_2SiCH_2CH_2$ (**2**), *n*-Hex (**3**), Ph (**4**); x = 0.55, R = $Et_3SiCH_2CH_2Si$ (**5**)] have been synthesized and their reactivity toward silver acetate examined in detail as a function of concentration of Ag(I) ions, polymer composition as well as side chain substituents on the polymers. A significant outcome of these studies is the isolation of polymer−silver nanocomposites which exhibit room temperature fluorescence characteristics as green light emitters in solution. This optical phenomenon is attributed to formation of silver nanoclusters in conjunction with nanoparticles in the organosilicon polymer scaffolds.

2. RESULTS AND DISCUSSION

2.1. Synthesis and Characterization of Polymers. Following Wurtz coupling approach,[2] the branched polysilanes $[(PhMeSi)_x\text{-}co\text{-}(RSi)_{1\text{-}x}]$ [x = 0.83−0.75, R = $Et_3SiCH_2CH_2$ (**1**), 2-$FuMe_2SiCH_2CH_2$ (Fu = furyl, **2**) *n*-Hex (**3**), Ph (**4**)] have been synthesized by reacting a mixture of dichloromethylphenylsilane and an appropriate trichloroorganosilane in 5:1 molar ratio with sodium dispersion in refluxing toluene. A change in the feed ratio of $Et_3SiCH_2CH_2SiCl_3$ and $PhMeSiCl_2$ monomers to 1:1 affords the polymer, $[(PhMeSi)_{0.55}\text{-}co\text{-}(Et_3SiCH_2CH_2Si)_{0.45}]_n$, **5**, with increased domains of branching sites. The synthesis of polysilyne $[Et_3SiCH_2CH_2Si]_n$, **6**, involves Wurtz coupling of trichlorocarbosilane, $Et_3SiCH_2CH_2SiCl_3$ as the precursor. Effective separation of high molecular weight polysilanes **1**−**6** from the reaction mixtures is performed by using 2-propanol as the precipitating solvent. These are obtained as white to pale yellow solids in 15−20% isolable yields. Gel permeation chromatographic analysis (THF, polystyrene standards) reveals a monomodal molecular weight distribution in each case with M_w/PDI values ranging between 9.7 and 21.0 × 10^3/PDI = 1.3−1.9 for **1**−**5** and 4.2/1.3 for **6** (Table1, Figure S1 (Supporting Information)). Thermogravimetric (TGA) studies suggest that all the polysilanes are thermally stable up to 290−300 °C. However, subsequent weight loss is observed in a continuous manner up to 500 °C leaving a residual yield of ∼30−40%. The ^{1}H NMR spectra of **1**−**3** and **5** are dominated by broad and overlapping resonances in the aliphatic region (δ 0.42−1.65) due to sila−alkyl/*n*-hexyl groups and assignments of chemical shifts are based on a comparison with those of related linear polysilanes reported earlier.[38] Nevertheless, quantitative $^{13}C\{^1H\}$ NMR spectra exhibit distinct signals due to various organic moieties associated with $[PhMeSi]_n$ and $[RSi]_n$ segments and delineate the composition of each polymer. The relevant NMR data are summarized in the Experimental Section. ^{29}Si NMR spectra (CPMAS) display characteristic resonances at δ −30 to −42 and −55 to −65 due to linear and branched sites respectively[1,32] (Figure 1). For **1**, **5** and **2**, the signals due to Et_3Si and $FuMe_2Si$ groups of the appended side chains appear at δ 8.7, 8.9, and −9.18 respectively. UV−vis spectra of **1**−**4** in toluene solution are quite similar and exhibit an absorption maximum in each case at ∼330 nm associated with $\sigma-\sigma^*$ transition of linear poly(methylphenylsilane) segment while a

Table 1. GPC Data of the Parent Polymers 1−6 and Oxidized Polymers[a]

	polymer	$M_w \times 10^{-3}$/PDI	composite	polymer: Ag(OAc)	$M_w \times 10^{-3}$/PDI
1	$[(PhMeSi)_{0.83}$-*co*-$(Et_3SiCH_2CH_2Si)_{0.17}]_n$	12.1/1.3	**1a**	0.10	9.87/2.1
			1b	0.25	4.85/2.0
			1c	0.50	-
2	$[(PhMeSi)_{0.80}$-*co*-$(2\text{-}FuMe_2SiCH_2CH_2Si)_{0.20}]_n$	9.8/1.9	**2a**	0.10	6.70/1.4
			2b	0.25	4.04/1.6
3	$[(PhMeSi)_{0.75}$-*co*-$(n\text{-}HexSi)_{0.25}]_n$	21.1/1.7	**3a**	0.10	10.43/1.5
			3b	0.25	6.91/2.3
4	$[(PhMeSi)_{0.82}$-*co*-$(PhSi)_{0.18}]_n$	10.3/1.5	**4a**	0.10	6.37/1.8
			4b	0.25	5.18/2.1
5	$[(PhMeSi)_{0.55}$-*co*-$(Et_3SiCH_2CH_2Si)_{0.45}]_n$	9.7/1.5	**5a**	0.10	-
6	$[Et_3SiCH_2CH_2Si]_n$	4.2/1.3	**6a**	0.10	-

[a] Molecular weights relative to polystyrene standards; eluent: THF; 30 °C. PDI = polydispersity index (M_w/M_n).

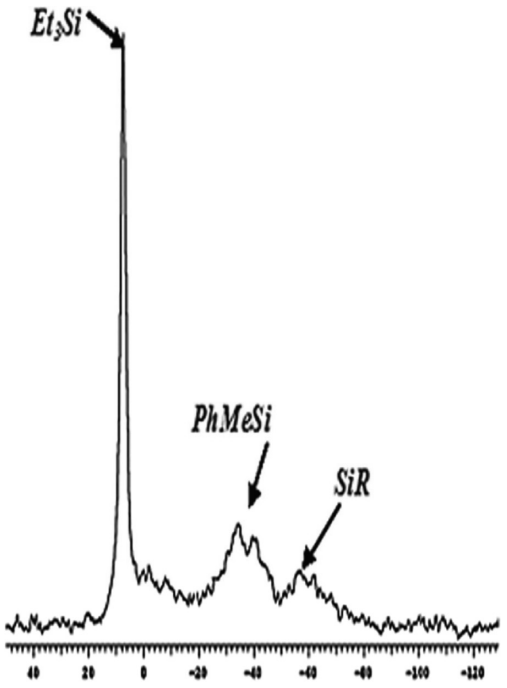

Figure 1. Solid state $^{29}Si\{^1H\}$ NMR spectrum of **1**.

shift to lower wavelength (318 nm) is observed in **5** as a result of increasing branching structures in the polymer framework.[38] The spectral profiles show an absorption edge to higher wavelength due to the presence of polysilyne units. In the photoluminescence (PL) spectra, the emission bands at 363−370 nm as well as several vibronic peaks at 407, 430, and 460 nm provide signatures of linear and branched segments, respectively. For **5**, PL emission bands associated with linear (361 nm) and branched polysilyne units show a perceptible variation in their intensities as compared to that of **1** suggesting higher order of branching and are in accord with those of analogous branched polysilanes reported earlier.[38,39] Strong evidence in favor of the network structure of **6** comes from $^{29}Si\{^1H\}$ NMR chemical shift [δ 8.36 (Et_3Si), −56 to −70 (br, backbone)] as well as PL emission bands at 407, 430, 460 nm. The polymers **1**, **2** and **6** have been chosen as representatives for cyclic voltammetric studies with Hg/Hg_2Cl_2 as the reference electrode. For **1** and **2**, the results reveal two distinct onsets of oxidation (V_i) at 0.84/0.89 and 0.36 V corresponding to linear poly(methylphenylsilane)[44] and polysilyne units[37] respectively while the polysilyne **6** shows an onset of oxidation at 0.35 V. In all cases, the cyclic voltammograms are found to be irreversible in nature.

2.2. Synthesis of Polymer−Silver Nanocomposites. Slow addition of a solution of each polymer, **1**−**4** in toluene into a stirred suspension of silver acetate (0.10 molar with respect to polymer repeat unit) in the same solvent separately results in a slow dissolution of the salt within 2−3 h. A gradual color change of the solutions from colorless to yellow during this period suggests the formation of silver nanoparticles (AgNPs) in each case. The reduction of Ag(I) to Ag(0) is accomplished by σ−delocalized electrons of the polysilanes and does not require any external reducing agent. Subsequent removal of the solvent from reaction mixtures under vacuum affords polymer-silver nanocomposites **1a**−**4a** respectively as orange solids. Similarly, the reactions of **1**−**4** with 0.25 molar concentration of silver acetate proceed in an identical manner to afford the composites, **1b**−**4b** respectively as sticky viscous mass, thereby suggesting that irreversible oxidative cleavage of the parent polymers is more pronounced in these cases as compared to those observed in **1a**-**4a** (Table 1). A detailed study on the compositional aspects of the polymer matrices in these composites is presented in section 2.2.2 (*vide infra*). All the nanocomposites thus obtained exhibit excellent chemical stability over a period of 3−4 months when stored in dark.

2.2.1. Characterization of Silver Nanoparticles/Clusters in the Composites. In view of slow agglomeration of silver nanoparticles in solution, relevant studies for the characterization of these composites have been performed on a freshly prepared solution in toluene. Transmission electron microscopy (TEM) reveals invariably the formation of spherical silver nanoparticles in a quasi-monodispersed phase with an average diameter of 5−7 nm for **1a**−**4a** and 8−11 nm for **1b**−**4b**, suggesting a perceptible increase in particle growth at higher concentration of Ag(I) ions in the reaction mixture. The representative TEM images of **1a** and **1b** are shown in Figure 2. Analysis of the crystal lattice shows Ag(1,1,1) with its characteristic 0.235−0.241 nm spacing.

As shown in Figure 3, UV−vis spectra of the nanocomposites (toluene, 10^{-4} M with respect to repeat unit of polymer) reveal surface plasmon resonance (SPR) at 427−433 nm due to silver nanoparticles, in addition to the absorption at 330 nm associated with $\sigma-\sigma^*$ electronic transition of linear poly(methylphenylsilane) segment. The absorption maxima of the plasmon resonance

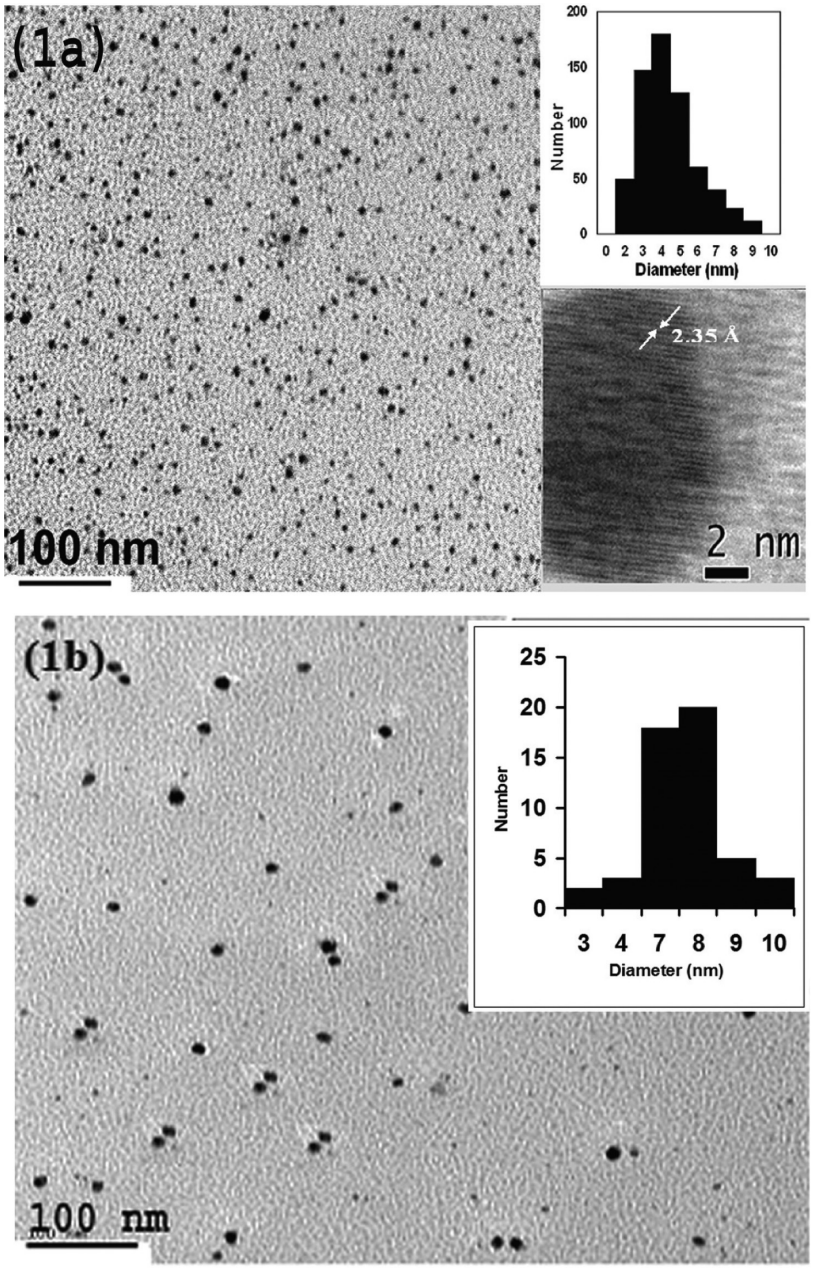

Figure 2. TEM images of polymer−Ag nanocomposites **1a** and **1b** with particle size distribution and HRTEM image of a large particle in the composite.

remain practically similar in all the composites and are found to be independent of nanosilver concentration or nature of side chain substituents in the host polymers. Nevertheless, the observed values are in accord with a few recent reports on related silver nanocomposites containing spherical silver nanoparticles of 2−5 nm diameter[10,45,46] as well as silver nanoclusters of Ag_2−Ag_8 dimensions,[16,27,28] thereby suggesting a strong dependence of the plasmon resonance on various parameters including size, shape, nature of capping agents and solvent medium.[47] A significant feature of the PL spectra (λ_{exc} = 350 nm) is the appearance of a new band at 515−550 nm in lieu of the emission bands associated with the polysilyne units of the parent polymers (Figure 4). The only exception to this behavior is observed in case of **3b** (Table 1) wherein the spectrum is dominated by the emission band at 360 nm due to linear poly(methylphenylsilane) only. The new emission is found to be independent of excitation wavelengths in the range of 350−430 nm (Figure S2, Supporting Information), thereby suggesting that the obtained emission is a real luminescence from the relaxed state and not due to scattering effect. This emissive behavior of the nanocomposites is corroborated by the observed green luminescence under UV light (inset, Figure 4). Confocal microscopy images of **1a** in 450−580 nm range (Figure S3, Supporting Information) suggest that highest intensity emission lies in λ scan region of 510−530 nm. The results obtained from photoluminescence spectra and fluorescent nature of each composite (except **3b**) as green light emitter provide a strong basis to suggest the formation of silver nanoclusters, in addition to the nanoparticles, as no plasmon emission is anticipated from bulk silver nanoparticles. Luminescence from small clusters on silver nanoparticle surfaces is rare but not unprecedentated.[19,26−28] Time-resolved fluorescence decay of the composite **1a** has been studied to substantiate the

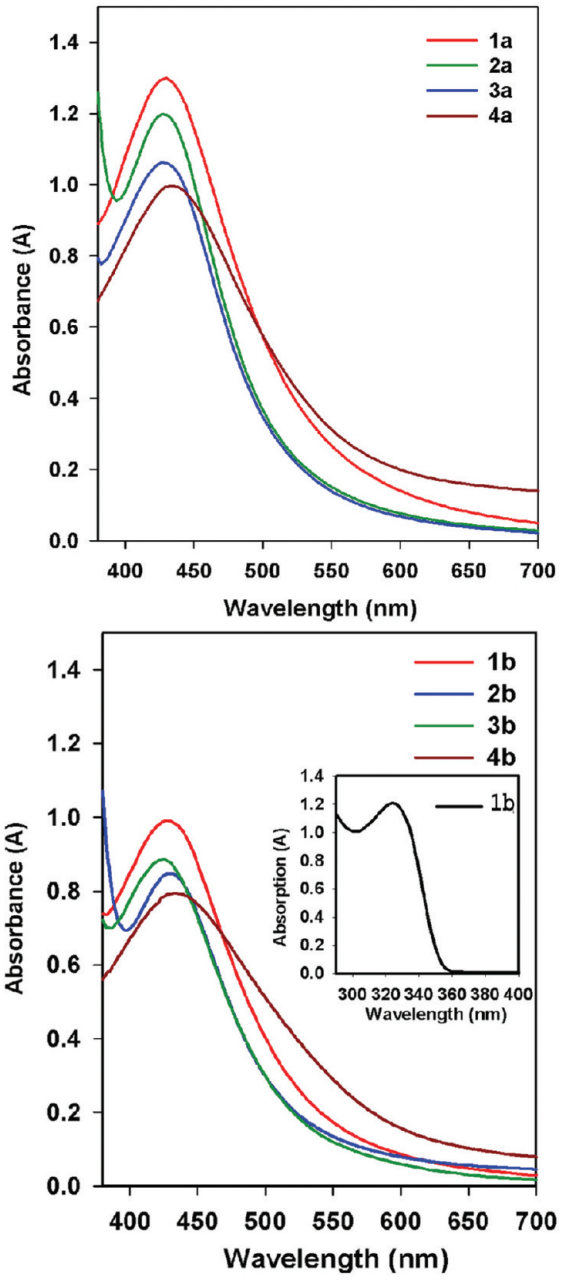

Figure 3. UV−vis spectra (toluene, room temperature, 7×10^{-4} M) showing surface plasmon resonance of Ag nanoparticles and $\sigma-\sigma^*$ transition of polymer (inset).

presence of silver nanoclusters. The decay phenomenon is monitored at 525 nm by using 340 nm lasers and instrument functions are shown in Figure 5. The result can be fitted biexponentially with a fast component of 409 ps (55%) and a slow component of 2.84 ns (45%). The former value is assigned to the host polymer matrix and the latter with longer lifetime is consistent with a few recent reports on Ag_2 clusters which reveal fluorescence lifetime of 2−3 ns.[19,22,23] The lifetime of fluorescence decay when detected at 363 nm [51 ps (98.83%) and 1.34 ns] is consistent with the results derived from the parent copolymer [44 ps (99.04%) and 1.35 ns] (Figure S4, Supporting Information).[48] The ESI−MS spectra of the composites have been recorded and the results are far from conclusive to establish the identity of Ag_2 and related small clusters. Nevertheless, the cluster peak at m/z 106.9 and 108.9 unequivocally reveal the presence of $[Ag]^+$ under the spectroscopic conditions. It is imperative to mention that there are only a few earlier reports on the mass spectral data on silver nanoclusters and identification of such species has been accounted for the composites possessing nanoparticles of <2 nm size.[16,18,25,29] In general, silver nanoclusters on the surface of nanoparticles have not been subjected to mass spectral studies.[19,26−28]

On the basis of these results, it is apparent that the branched organosilicon polymers are versatile scaffolds for the generation and stabilization of silver nanoparticles as well as nanoclusters as fluorophores. As a result, possible interaction between nanoparticle−nanocluster interface which may result in fluorescence enhancement/quenching in the composites, **1a**−**4a** and **1b**−**4b** cannot be discounted. However, a detailed study of such phenomena is warranted in view of paucity of literature precedence, although recent studies on the optical properties of organic fluorophores in the viscinity of silver nanoparticles are emerging.[49] A plausible explanation of the observed variations in the relative intensity of emission bands at 515−550 nm (Figure 4) is provided by considering nature of the host polymers bearing different side chain substituents as well as concentration of silver nanoparticles in the composites. These effects are particularly noticeable in case of composite **3b** wherein the absence of fluorescence characteristics may result from instability of nanoclusters due to long *n*-hexyl groups in the host polymer as well as higher concentration of silver nanoparticles. The effect of silver concentration on the optical properties of the composites has been further validated by studying UV−vis and PL spectra of the composite, **1c** (Table 1) which has been isolated from reaction of polymer **1** with 0.5 molar concentration of silver acetate. In this case, although the plasmon resonance due to silver nanoparticles is discernible at λ_{max}= 420 nm, the PL spectrum is devoid of the emission band at 530 nm region suggesting the absence of silver nanoclusters (Figure S5, Supporting Information). The composite is poorly stable and precipitation of silver nanoparticles is observed within 48 h. It is believed that extensive cleavage of the parent polymer during the conversion of Ag(I) to Ag(0) results in the formation of a matrix comprising of mainly oligosilanes which do not act as scaffolds to stabilize the nanoparticles.

2.2.2. Compositional Aspects of Host Polymer Matrices and Their Relevance in the Stabilization of Silver Nano Clusters. The host polymer matrices are isolated from the composites by addition of a donor solvent such as THF which results in agglomeration and precipitation of the metal nanoparticles. These polymers are obtained as white solids or viscous mass and the GPC data (Table 1, Figure S6 (Supporting Infomation)) reveal a perceptible decrease in molecular weights (M_w = 10.4−4.8 $\times$ 10^3) as compared to the corresponding parent polymers. It is noteworthy that the oxidative cleavage of silicon backbone is more pronounced in case of the polymers derived from **1b**−**4b** composites. The reduction of Ag(I) ions to Ag(0) results in the inclusion of siloxane groups in each polymer matrix and its presence is established by a new intense broad IR absorption at 1060−1080 cm^{-1}. The results are consistent with earlier reports on the reducing behavior of linear polysilanes toward Ag(I) ions.[13,6−8]

UV−vis and PL spectra of these polymers identify linear polysilane segment by characteristic absorption and emission bands at 330 and 360−365 nm, respectively. The position of the absorption/emission maximum does not reveal any perceptible

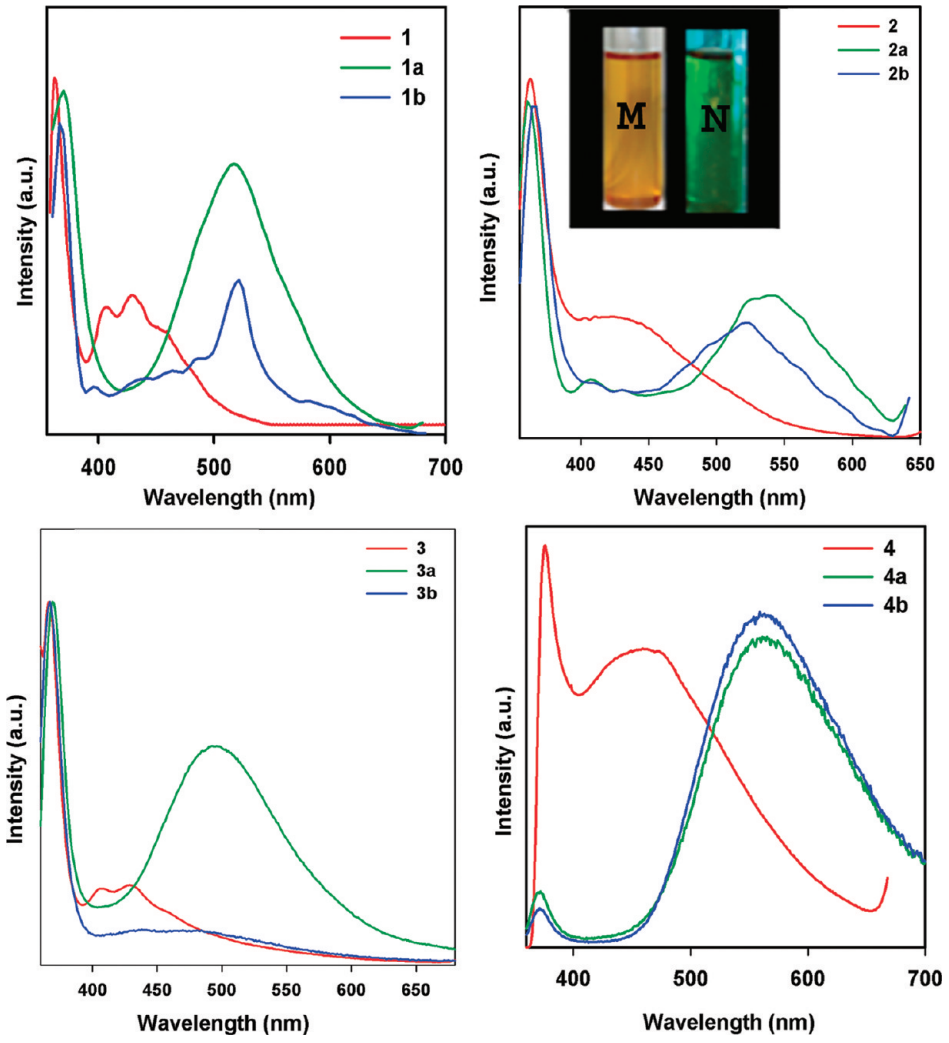

Figure 4. Emission spectra (λ_{exc} = 350 nm, toluene, room temperature) of nanocomposites. The inset shows the composite solution in room light (**M**) and UV light (**N**).

change in comparison to that of the corresponding parent polymer. Nevertheless, PL spectra in the polysilyne region (λ_{max} = 450 nm) differ appreciably as compared to those of the composites as well as the parent polysilanes (Figure 4). The spectral profiles of the host polymer matrices derived from **1a**−**4a** exhibit the signatures of residual polysilyne fragments while those isolated from **1b**−**4b** are devoid of this characteristic emission (Figure 6). In addition, the spectra of all these polymers invariably show the absence of emission band at 525 nm as observed in the composites. These results provide the basis to draw a few important conclusions: (a) The absence of polysilyne units in the host polymers derived from **1b**−**4b** clearly suggest that these act as preferential sites for the reduction of Ag(I) ions to Ag(0) in comparison to the linear polymethylphenylsilane segment. A plausible explanation of this behavior is sought by cyclic voltammetric study (Figure 7) of the host polymers derived from the composites **1a** and **1b** and comparing the results with that of parent polymer **1**. It is evident that the cyclic voltammogram of the host polymer obtained from the composite **1a** closely resembles that of the parent polymer and exhibit two distinct, irreversible onsets of oxidation (V_i) at 0.84 and 0.36 V due to linear polysilane and polysilyne units, respectively. On the other hand, the host polymer matrix derived from **1b** does not exhibit the peak at 0.36 V due to branched polysilyne units. (b) The green emission at 525 nm and associated fluorescence characteristics of the composites are the attributes of Ag nanoparticles and do not originate from the polymer matrices.

To better understand the compositional effects of these polymers on the stability of silver nanoparticles/clusters, the reactions of $[(PhMeSi)_{0.55}\text{-}co\text{-}(Et_3SiCH_2CH_2Si)_{0.45}]_n$, **5**, and $[Et_3SiCH_2CH_2Si]_n$, **6**, with 0.10 equiv of silver acetate have been performed to afford the isolation of polymer-silver nanocomposites **5a** and **6a** respectively. Needless to mention that the former is an analogue of the polymer **1** (Table 1) with increasing branching sites while the latter is comprised of a network structure. Preliminary studies based on TEM, UV−vis and PL spectroscopy and comparison of the results with those of **1a** have revealed a few interesting observations. The TEM images of **5a** and **6a** (Figure S7, Supporting Information) reveal that the silver nanoparticles are quite large and polydispersed in nature (8.5 ± 5.2 nm/14 ± 6.16 nm) as compared to those formed in the composite **1a**. Although absorption maxima of the surface plasmon resonances of silver nanoparticles (435 nm for **5a**; 425 nm for **6a**) resemble closely, a marked variation in the

dx.doi.org/10.1021/ma200038x |*Macromolecules* 2011, 44, 3240–3249

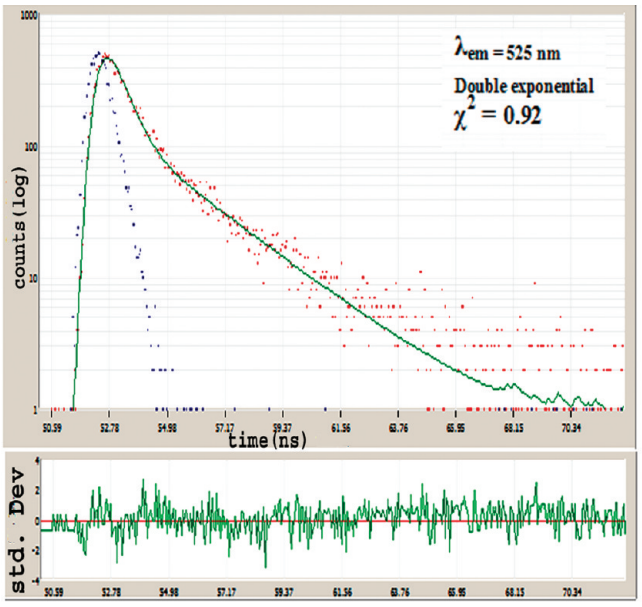

Figure 5. Fluorescence decay curve of nanocomposite **1a** monitored at 525 nm. Excitation is carried out by using 340 nm lasers. The bottom curves (blue) denote the instrumental response function, the top panels (green) provide double-exponential fits to experimental data and the lower panels show weighted residuals for the corresponding fits.

emission bands is quite distinct in the photoluminescence spectra. As shown in Figure S8, Supporting Information, the spectrum of **5a** reveals the green emission at 516 nm similar to that observed in **1a**, the composite **6a** is devoid of this emission band. This difference in the emissive character implies that compositional features of the host polymers as well as size distribution of the *in situ* generated silver nanoparticles play a dominant role in the green light emission of polymer metal nanocomposites. In addition the reaction of a mixture of homopolymers $[PhMeSi]_n$ and $[Et_3SiCH_2CH_2Si]_n$ (5:1 equiv) with 0.10 equiv of silver acetate has been performed under identical conditions. The formation of silver nanoparticles of average diameter, 12.75 ± 4.02 nm is evident from TEM image while UV−vis spectrum exhibits a distinct surface plasmon resonance at 425 nm. Nevertheless, the nanocomposite thus formed does not exhibit fluorescent characteristics and is devoid of emission band at 525 nm (Figure S9, Supporting Information) in a range of excitation wavelengths between 350 to 430 nm. These studies clearly suggest that the polymer matrix derived from physical blend of the homopolymers does not meet the structural requirements which are essential for the protection of *in situ* generated silver nanoclusters.

In summary we have demonstrated that the branched polysilanes **1**−**5** undergo a facile reaction with silver acetate to afford silver nanocomposites which are fluorescent as a result of formation of silver nanoclusters. The preferential site of reduction of Ag(I) ions is located in the polysilyne segment of these polymers resulting in chemical modifications via oxidative cleavage of the silicon backbone and formation of Si−O−Si linkages. The host polymers with linear polysilane and siloxane containing branching units in the structural frameworks act as templates for stabilization of silver nanoclusters owing to their complex two-dimensional network architecture. The legacy of these branched organosilicon polymers to exhibit two distinct oxidation potentials associated with linear and branched segments of the skeletal silicon backbone, may have significant implications in synthesis of hybrid noble metal nanoparticles.

3. EXPERIMENTAL SECTION

3.1. General Comments. All operations were carried out using standard Schlenk line techniques under dry nitrogen atmosphere unless otherwise stated. Solvents were freshly distilled under inert atmosphere over sodium/benzophenone (toluene, tetrahydrofuran) and magnesium (alcohols) before use. Trichlorovinylsilane, *n*-hexyltrichlorosilane and phenyltrichlorosilane (Aldrich) were freshly distilled over magnesium. Karstedt's catalyst (platinum(0)-1,3-divinyl-1,1,3,3-tetramethyldisiloxane complex), and silver acetate (Aldrich) were used as received. Molecular weights of the polysilanes were estimated using Hitachi ELITE LaChrom chromatograph equipped with L-2490 refractive index detector and Waters styragel HR3 and HR4 columns in series. The chromatograph was calibrated with polystyrene standards and THF was used as eluent. UV−vis spectra were recorded on a Perkin-Elmer (Lambda Bio 20) spectrophotometer. Fluorescence spectra were acquired on model FL 3-11, Fluorolog-3 modular spectrofluorometer purchased from Horoba-Jobin Yvon, Inc. The spectrofluorometer contains single Czerny-Turner grating excitation and emission monochromators as wavelength selection devices, 450 W Xe-arc lamps as the excitation source and PMT as the detector. ^1H and ^{13}C NMR spectra were recorded in $CDCl_3$ on Bruker Spectrospin DPX 300 MHz instrument at frequency 300 and 75.5 MHz respectively while ^{29}Si spectra were recorded on Bruker AVANCE II 400 NMR spectrometer at frequency 79.5 MHz and chemical shifts are quoted relative to Me_4Si. Thermogravimetric analysis of polymers was carried out in nitrogen atmosphere between 50 and 900 °C at a rate of 10 °C/min on a Perkin-Elmer Thermal analysis system. Infrared spectra were obtained on a Nicolet FT-IR (protege) spectrometer using KBr optics. Transmission electron microscopic (TEM) studies were carried out on a FEI Technai G2 electron microscope operated at 200 kV. The diameter of the particles from the TEM images was calculated using image processing software, Image J. TEM samples were prepared by depositing one drop of the silver nanoparticles solution on a carbon coated copper grid and allowing the solvent to evaporate. Cyclic voltammetric measurements were carried out on μAutolab type-III Potensiostat/Galvanostat electrochemical analyzing system. The scan rate employed was 5 mV/s. Cyclic voltammograms were recorded in THF with 0.2 M anhydrous $LiClO_4$ as supporting electrolyte. A three-electrode set up comprising of a Pt disk working electrode (surface area =0.8 × 1.0 cm^2), a Pt wire counter electrode and Hg/Hg_2Cl_2 as reference electrode was used. The polymer solutions were prepared in a concentration of ~5 mg/mL. Inverted Olympus FV-1000 confocal laser scanning microscope was used for scanning the images in the λ scan region of 450−580 nm. The mass spectrum was recorded on a micrOTOF-Q II 10262 mass spectrometer in positive ion mode by ESI technique. The assignment of the observed fgragment ion has been made by using the Chem Draw Ultra 7.0.1 program.

3.2. Synthetic Methods. *Synthesis of $Et_3SiCH_2CH_2SiCl_3$.* Triethylsilane (6.2 mL, 39 mmol) was added dropwise into a stirred solution of trichlorovinylsilane (5 mL, 39 mmol) containing Karstedt's catalyst. Strong induction period was observed after a few drops of addition of triethylsilane. The reaction mixture was heated at 90 °C for 10−12 h and subsequently fractionally distilled under vacuum to afford the title compound as a colorless liquid. (bp 100−105 °C/5 mm Hg; yield 72%). ^1H NMR ($CDCl_3$, 300 MHz): δ 1.29−1.23 (m, CH_2SiCl_3, 2H), 1.0−0.94 (t, CH_3−Et, 9H), 0.76−0.68 (m, Et_3SiCH_2, 2H), 0.57−0.46 (q, CH_2−Et, 6H). $^{29}Si\{^1H\}$ NMR ($CDCl_3$, 79.5 MHz): δ 8.94 (Et_3Si), 13.36 ($SiCl_3$).

Synthesis of 2-$FuMe_2SiCH_2CH_2SiCl_3$. The synthesis of $FuMe_2SiH$ was carried out by the following procedure reported earlier using salt elimination reaction between furyllithium and chlorodimethylsilane.[50]

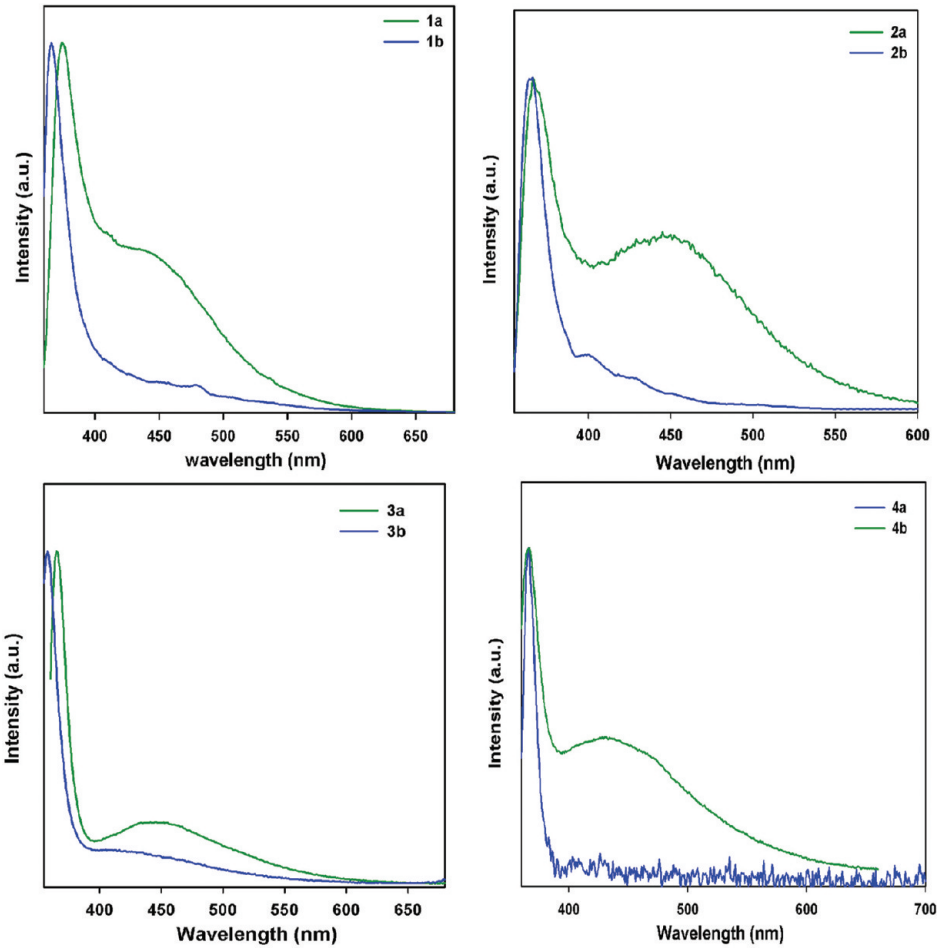

Figure 6. Emission spectra (λ_{exc} = 350 nm, toluene, room temperature) of the oxidized polymer matrices.

Hydrosilylation reaction between trichlorovinylsilane (5.5 mL, 40 mmol) and dimethyl(2-furyl)silane (5 g, 39 mmol) was carried out in presence of Karstedt's catalyst. The contents were refluxed at 90 °C for 10−12 h to ensure completion of the reaction and thereafter fractionally distilled under vacuum to afford the desired trichlorocarbosilane. (bp 140−145 °C/5 mm Hg; yield 70%). ^{1}H NMR ($CDCl_3$, 300 MHz): δ 7.59 (d, $^3J_{HH}$ = 1.5 Hz, *Fu* H-5), 6.63 (dd, $^3J_{HH}$ = 3 Hz, $^3J_{HH}$ = 3.21 Hz, *Fu* H-3), 6.32 (d, $^3J_{HH}$ = 1.14 Hz, *Fu* H-4), δ 1.17−1.26 (m, CH_2SiCl_3, 2H), 0.81−0.87 (m, $FuMe_2SiCH_2$, 2H), 0.22 (s, Si−Me, 6H). ^{29}Si{^{1}H} NMR ($CDCl_3$, 79.5 MHz): δ −8.56 ($FuMe_2Si$), 13.46 ($SiCl_3$).

Synthesis of Branched Polysilanes ***1***−***5***. A typical procedure for the synthesis of branched polysilanes, **1**−**4** is as follows. Freshly weighed sodium (1.8 g, 78.2 mmol) was transformed to a fine dispersion in refluxing toluene under dry nitrogen atmosphere and a solution of dichloromethylphenylsilane (4.70 g, 4.0 mL, 24.60 mmol) and trichlorosilane precursor, $Et_3SiCH_2CH_2SiCl_3$ (1.36 g, 4.90 mmol) was added dropwise into it (*Caution! a strongly exothermic reaction occurs*). The reaction mixture turned deep blue in color, and the contents were allowed to reflux at 110 °C for 4 h. The resulting solution was then filtered under nitrogen and the solvent was stripped off from the filtrate to afford a crude polymer. The high molecular weight branched polysilane **1** was obtained as a white solid by repeated fractionation of a concentrated solution of crude product in toluene using 2-propanol as the precipitating solvent. Following a similar procedure, the branched polysilanes **2**−**4** were obtained as white solids by reacting a mixture of dichloromethylphenylsilane and $FuSiCH_2CH_2SiCl_3$/*n*-$HexSiCl_3$/$PhSiCl_3$ in 5:1 molar ratio under Wurtz coupling condition. Following a similar procedure, the branched polysilane **5** was obtained as yellowish solid by reacting equimolar quantity of dichloromethylphenylsilane (2.35 g, 2.0 mL, 12.30 mmol) and trichlorosilane precursor $Et_3SiCH_2CH_2SiCl_3$ (3.41 g, 12.30 mmol) with sodium dispersion (1.69 g, 73.47 mmol).

[(PhMeSi)$_{0.83}$-co-(Et$_3$SiCH$_2$CH$_2$Si)$_{0.17}$]$_n$, *1*. Yield = 16.5%. GPC: M_w = 12096; PDI = 1.3. ^{1}H NMR ($CDCl_3$, 300 MHz): δ 7.28 (br, Si−*Ph*), 0.82 (br, CH_3−Et), 0.28 (br, CH_2 + CH_2−Et), −0.20 (br, Si*Me*). ^{13}C{^{1}H} NMR ($CDCl_3$, 75.5 MHz): δ 135.13, 133.33, 127.61 (Si−*Ph*), 11.64 (CH_2Si), 7.52 (CH_3−Et), 6.16 (Et_3SiCH_2), 2.75 (CH_2−Et), −6.13 (Si*Me*). ^{29}Si{^{1}H} NMR (solid): δ 8.70 (Et_3Si), −32 to −40 (br, PhMe*Si*), −56 to −65 (br, polysilyne backbone). IR (KBr, cm^{-1}): 3055 (Ar, ν_{C-H}), 2951, 2878 (ν_{C-H}), 1248 (ν_{Si-Me}), 1418 (δ_{C-H}). UV−vis (λ_{max}) = 331 nm. PL (λ_{max}) = 363 nm (linear polysilane segment) and 407, 430, and 460 nm (polysilyne segment)

[(PhMeSi)$_{0.80}$-co-(2-FuMe$_2$SiCH$_2$CH$_2$Si)$_{0.20}$]$_n$, *2*. Yield = 15.8%. GPC: M_w = 9769; PDI = 1.9. ^{1}H NMR ($CDCl_3$, 300 MHz): δ 7.27 (br, Si−*Ph*, Si−*Fu*), 0.77 (br, CH_2 + CH_2Si + Fu*Me*$_2$), 0.12 (Si*Me*). ^{13}C{^{1}H} NMR ($CDCl_3$, 75.5 MHz): δ 135.02, 133.29, 129.56, 128.99, 127.67 (Si−*Ph*, Si−*Fu*), 14.56 (CH_2Si), 7.34 (Me_2SiCH_2), −4.01 (Fu*Me*$_2$), −6.34 (Si*Me*). ^{29}Si{^{1}H} NMR (solid): δ −9.18 ($FuMe_2Si$) −39 to −42 (br, PhMe*Si*), −55 to −65 (br, polysilyne backbone). IR (KBr, cm^{-1}): 3116 (Ar, ν_{C-H}), 2961, 2894 (ν_{C-H}), 1256 (ν_{Si-Me}), 1421 (δ_{C-H}). UV−vis (λ_{max}) = 327 nm. PL (λ_{max}) = 363 nm (linear polysilane segment) and 450 nm (br, polysilyne segment).

[(PhMeSi)$_{0.75}$-co-(n-HexSi)$_{0.25}$]$_n$, *3*. Yield = 18.5%. GPC: M_w = 21078; PDI = 1.7. ^{1}H NMR ($CDCl_3$, 300 MHz): δ 7.17 (br, Si−*Ph*), 1.65 (br,

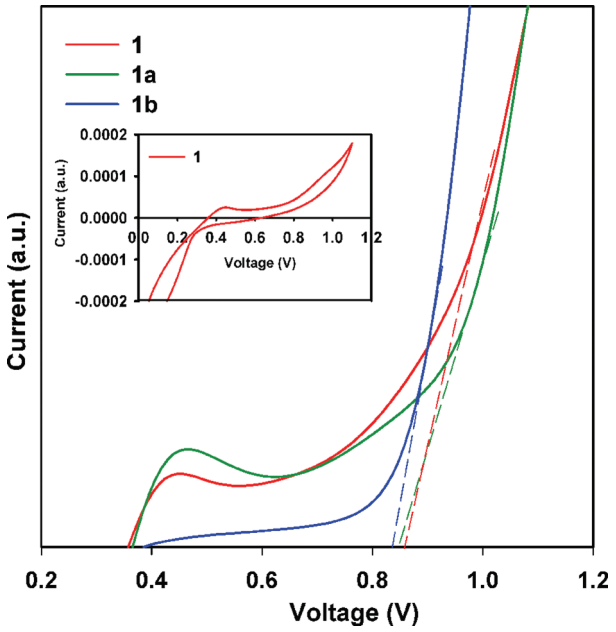

Figure 7. Cyclic voltammograms showing oxidation wave of polymer **1** and the oxidized polymer matrices from the composites **1a** and **2a** (inset: full CV profile of 1). Supporting electrolyte: 0.2 M $LiClO_4$. Electrodes: Pt vs Hg/Hg_2Cl_2. Scan rate: 5 mV/s. Dashed lines are tangents to determine the onset of oxidation potential.

H_2-H_5), 1.14 (br, H_1/H_6), 0.79 (br, Si*Me*). $^{13}C\{^1H\}$ NMR ($CDCl_3$, 75.5 MHz): δ 135.02, 133.27, 127.44 (Si*Ph*), 33.59, 31.29, 29.72, 22.54, 19.41, 14.10 (Si*Hex*), −6.89 (Si*Me*). $^{29}Si\{^1H\}$ NMR (solid): δ −39 to −43 (br, PhMe*Si*), −55 to −65 (br, polysilyne backbone). IR (KBr, cm^{-1}): 3045(Ar, ν_{C-H}), 2953, 2851(ν_{C-H}), 1243 (ν_{Si-Me}), 1423 (δ_{C-H}). UV−vis (λ_{max}) = 330 nm. PL (λ_{max}) = 366 nm (linear polysilane segment) and 407, 430, and 460 nm (polysilyne segment).

[(PhMeSi)$_{0.82}$-co-(PhSi)$_{0.18}$]$_n$, *4*. Yield = 19.5%. GPC: M_w = 10260; PDI = 1.5. UV−vis (λ_{max}) = 332 nm, PL (λ_{max}) = 370 nm (linear polysilane segment), 450 nm (br, polysilyne segment). These results are in accord with those reported earlier.[38]

[(PhMeSi)$_{0.55}$-co-(Et$_3$SiCH$_2$CH$_2$Si)$_{0.45}$]$_n$, *5*. Yield = 14.7%. GPC: M_w = 9726; PDI = 1.6. ^1H NMR ($CDCl_3$, 300 MHz): δ 7.18 (br, Si−*Ph*), 0.85 (br, C*H*$_3$−Et), 0.42 (br, SiC*H*$_2$ + C*H*$_2$−Et), 0.30 (br, Si*Me*). $^{13}C\{^1H\}$ NMR ($CDCl_3$, 75.5 MHz): δ 135.23, 133.34, 127.65 (Si−*Ph*), 11.60 (*C*H$_2$Si), 7.01 (*C*H$_3$−Et), 6.12 (Et$_3$SiCH$_2$), 2.86 (*C*H$_2$−Et), −3.68 (Si*Me*). $^{29}Si\{^1H\}$ NMR (solid): δ 8.9 (Et$_3$*Si*), −30 to −40 (br, PhMe*Si*), −55 to −65 (br, polysilyne backbone). IR (KBr, cm^{-1}): 3055 (Ar, ν_{C-H}), 2950, 2875 (ν_{C-H}), 1238 (ν_{Si-Me}), 1417 (δ_{C-H}). UV−vis (λ_{max}) = 318 nm. PL (λ_{max}) = 360 nm (linear polysilane segment) and 407, 430, and 460 nm (polysilyne segment).

Synthesis of Homopolymers. For the synthesis of polysilyne [Et$_3$SiCH$_2$CH$_2$Si]$_n$, **6**, trichlorocarbosilane precursor Et$_3$SiCH$_2$CH$_2$SiCl$_3$ (5 g, 18.0 mmol) was reacted with sodium dispersion in refluxing toluene (20 mL). After heating the content for 4 h, the salt was filtered to obtain a yellow solution. The filtrate thus obtained was concentrated and 2-propanol was added to precipitate a yellow solid. The procedure was repeated 2−3 times to obtain the high molecular weight polysilyne. Yield =14.4%, GPC: M_w = 4153; PDI = 1.3. ^1H NMR ($CDCl_3$, 300 MHz): δ 0.87 to 1.10 (br, C*H*$_2$ + C*H*$_2$−Et), 0.31 to 0.45 (br, C*H*$_3$−Et). $^{13}C\{^1H\}$ NMR ($CDCl_3$, 75.5 MHz): 12.23 (*C*H$_2$Si), 7.47 (*C*H$_3$−Et), 6.55 (Et$_3$SiCH$_2$), 2.87 (*C*H$_2$−Et). $^{29}Si\{^1H\}$ NMR (solid): δ 8.52 (Et$_3$Si), −55 to −70 (br, polysilyne backbone).

As reported earlier,[51] poly(methylphenylsilane) was obtained by following Wurtz coupling reaction using dichloromethylphenylsilane as the precursor. Relevant spectroscopic data of the polysilane obtained herein is given as follows. GPC: M_w =21344; PDI = 1.5. UV−vis (λ_{max}) = 340 nm. PL (λ_{max}) = 367 nm.

Synthesis of Polymer−Silver Nanocomposites. The synthetic protocol for the nanocomposites is similar in all cases. A typical procedure is described as follows. To a stirred suspension of silver acetate (19.0 mg, 0.11 mmol) in toluene (35 mL, HPLC grade), a solution of polysilanes **1**−**4** (1.14 mmol with respect to polymer repeat unit) in the same solvent was added separately under aerobic conditions. Slow dissolution of silver acetate was observed in each case and a clear yellow solution was obtained after 2−3 h, which was centrifuged at 2000 rpm in order to remove any traces of unreacted silver acetate. The solvent was removed under vacuum yielding pale orange solids which were identified as the composites **1a**−**4a** respectively. Following a similar procedure, the isolation of the composites **1b**−**4b** was achieved from the reaction of silver acetate (47.7 mg, 0.28 mmol) with the corresponding branched polysilanes, **1**−**4**. These are isolated as orange colored viscous mass. The isolation of the composites **5a** and **6a** was effected in a similar manner by reacting **5** (0.15 g, 1.03 mmol) or **6** (0.18 g, 1.03 mmol) with 0.1 equiv of silver acetate (17.2 mg, 0.10 mmol) in toluene (35 mL, HPLC grade).

Synthesis of Polymer−Silver Nanocomposites from the Homopolymers [Et$_3$SiCH$_2$CH$_2$Si]$_n$ and [PhMeSi]$_n$. A solution containing a mixture of [PhMeSi]$_n$ (28.80 mg, 0.24 mmol) and [Et$_3$SiCH$_2$CH$_2$Si]$_n$ (10.26 mg, 0.06 mmol) in toluene (HPLC grade) was added to a stirred suspension of silver acetate (5.0 mg, 0.03 mmol) in toluene (20 mL). Slow dissolution of silver acetate was observed and a clear yellow solution was obtained after 3−4 h which was centrifuged at 2000 rpm. The resulting solution containing silver nanoparticles was used for UV−vis, PL, and TEM studies.

■ ASSOCIATED CONTENT

Supporting Information. Figures S1-S9 showing GPC profiles of branched polysilanes **1**−**6**, emission spectra of nanocomposites **1a** and **4a** at different excitation wavelengths, confocal microscopic images of composite **1a**, fluorescence lifetime decay of polymer **1** and **1a** monitored at 363 nm, UV/vis and PL emission spectra of silver nanocomposite **1c**, GPC profiles of oxidized polymers derived from composites **1a**−**4a** and **1b**−**4b**, TEM images of silver nanoparticles in composites **5a** and **6a**, PL emission of polymer **5** and composite **5a**, and emission spectra of Ag nanocomposite derived from mixture of homopolymers [PhMeSi]$_n$ and [Et$_3$SiCH$_2$CH$_2$Si]$_n$ at different excitation wavelengths. This material is available free of charge via the Internet at http://pubs.acs.org.

■ AUTHOR INFORMATION

Corresponding Author

*E-mail: shankar@chemistry.iitd.ac.in.

■ ACKNOWLEDGMENT

This research was supported by financial grant (Project No. SR/S1/IC-25/2007) from DST (India). We thank CSIR (India) for a fellowship to U.S. We are also grateful to Dr. Vijay Prakash for providing facility for cyclic voltammetry, Dr. Sidharth Pandey for fluorescence decay, and Dr. Sameer Sapra for helpful discussion.

■ REFERENCES

(1) Michl, J.; West, R. In *Silicon-Containing Polymers: The Science and Technology of Their Synthesis and Applications*; Jones, R. G., Ando,W., Chojnowski, J., Eds.; Kluwer, Dordrecht: The Netherlands, 2000; p 499.

(2) Miller, R. D.; Michl, J. *Chem. Rev.* **1989**, *89*, 1359–1410.
(3) Fukushima, M.; Noguchi, N.; Aramata, M.; Hamada, Y.; Tabei, E.; Mori, S.; Yamamoto, Y. *Synth. Met.* **1998**, *97*, 273–280.
(4) Ueno, M.; Suzuki, T.; Naito, T.; Oyamada, H.; Kobayashi, S. *Chem. Commun.* **2008**, 1647–1649.
(5) Oyamada, H.; Akiyama, R.; Hagio, H.; Naito, T.; Kobayashi, S. *Chem. Commun.* **2006**, 4297–4299.
(6) Oyamada, H.; Naito, T.; Miyamoto, S.; Akiyama, R.; Hagio, H.; Kobayashi, S. *Org. Biomol. Chem.* **2008**, *6*, 61–65.
(7) Sakurai, H. *Proc. Jpn. Acad., Ser. B* **2006**, *82*, 257–269.
(8) Sanji, T.; Ogawa, Y.; Nakatsuka, Y.; Tanaka, M.; Sakurai, H. *Chem. Lett.* **2003**, 980–981.
(9) Tamai, T.; Watanabe, M.; Hatanaka, Y.; Tsujiwaki, H.; Nishioka, N.; Matsukawa, K. *Langmuir* **2008**, *24*, 14203–14208.
(10) Chauhan, B. P. S.; Sardar, R. *Macromolecules* **2004**, *37*, 5136–5139.
(11) Weller, H. *Angew. Chem., Int. Ed. Engl.* **1993**, *32*, 41–53.
(12) Schmidt, G. *Chem. Rev.* **1992**, *92*, 1709–1727.
(13) Shankar, R.; Shahi, V.; Sahoo, U. *Chem. Mater.* **2010**, *22*, 1367–1375.
(14) Shankar, R.; Shahi, V. *J. Organomet. Chem.* **2008**, *693*, 307–315.
(15) Shankar, R.; Shahi, V. *J. Polym. Sci., Part A: Polym. Chem.* **2008**, *46*, 7816–7826.
(16) Zheng, J.; Dickson, R. M. *J. Am. Chem. Soc.* **2002**, *124*, 13982–13983.
(17) Xu, H.; Suslick, K. S. *Adv. Mater.* **2010**, *22*, 1078–1082.
(18) Diez, I.; Pusa, M.; Kulmala, S.; Jiang, H.; Walther, A.; Goldmann, A. S.; Muller, A. H. E.; Ikkala, O.; Ras, R. H. A. *Angew.Chem., Int. Ed.* **2009**, *48*, 2122–2125.
(19) Maretti, L.; Billone, P. S.; Liu, Y.; Scaiano, J. C. *J. Am. Chem. Soc.* **2009**, *131*, 13972–13980.
(20) Rabin, I.; Schulze, W.; Ertl, G. *J. Chem. Phys.* **1998**, *108*, 5137–5142.
(21) Lee, T. H.; Gonzalez, J. I.; Zheng, J.; Dickson, R. M. *Acc. Chem. Res.* **2005**, *38*, 534–541.
(22) Vosch, T.; Antoku, Y.; Hsiang, J. C.; Richards, C. I.; Gonzalez, J. I.; Dickson, R. M. *Proc. Natl. Acad. Sci. U.S.A.* **2007**, *104*, 12616–12621.
(23) Fedrigo, S.; Harbich, W.; Buttet, J. *J. Chem. Phys.* **1991**, *99a*, 5712–5717.
(24) Yu, J.; Choi, S.; Dickson, R. M. *Angew. Chem., Int. Ed.* **2009**, *48*, 318–320.
(25) Yu, J.; Patel, S. A.; Dickson, R. M. *Angew. Chem., Int. Ed.* **2007**, *46*, 2028–2030.
(26) Shen, Z.; Duan, H.; Frey, H. *Adv. Mater.* **2007**, *19*, 349–352.
(27) Zhang, J.; Xu, S.; Kumacheva, E. *Adv. Mater.* **2005**, *17*, 2336–2340.
(28) Shang, L.; Dong, S. *Chem. Commun.* **2008**, 1088–1090.
(29) Adhikari, B.; Banerjee, A. *Chem. Mater.* **2010**, *22*, 4364–4371.
(30) Petty, J. T.; Zheng, J.; Hud, N. V.; Dickson, R. M. *J. Am. Chem. Soc.* **2004**, *126*, 5207–5212.
(31) Bianconi, P. A.; Weidman, T. W. *J. Am. Chem. Soc.* **1988**, *110*, 2342–2344.
(32) Furukawa, K.; Fujino, M.; Matsumoto, N. *Macromolecules* **1990**, *23*, 3423–3426.
(33) Bianconi, P. A.; Schilling, F. C.; Weidman, T. W. *Macromolecules* **1989**, *22*, 1697–1704.
(34) Vink, R. L. C.; Barkema, G. T.; Walree, C. A. V.; Jenneskens, L. W. *J. Chem. Phys.* **2002**, *116*, 854–859.
(35) Fujiki, M.; Kawamoto, Y.; Kato, M.; Fujimoto, Y.; Saito, T.; Hososhima, S.; Kwak, G. *Chem. Mater.* **2009**, *21*, 2459–2466.
(36) Fukao, S.; Fujiki, M. *Macromolecules* **2009**, *40*, 8062–8067.
(37) Cleij, T. J.; Stellar Tsang, K. Y.; Jenneskens, L. W. *Macromolecules* **1999**, *32*, 3286–3294.
(38) Watanabe, A.; Miike, H.; Tsutsumi, Y.; Matsuda, M. *Macromolecules* **1993**, *26*, 2111–2116.
(39) Walree, C. A.; Cleij, T. J.; Jenneskens, L. W.; Vlietstra, E. J. *Macromolecules* **1996**, *29*, 7362–7373.
(40) Brus, L. *J. Phys. Chem.* **1994**, *98*, 3575–3581.
(41) Fiedler, U. J.; Kockerling, M.; Reinke, H.; Krempner, C. *Chem. Commun.* **2010**, *46*, 4535–4537.
(42) Zhou, Z.; Brus, L.; Friesner, R. *Nano Lett.* **2003**, *3*, 163–167.
(43) Zhou, Z.; Friesner, R. A.; Brus, L. *J. Am. Chem. Soc.* **2003**, *125*, 15599–15607.
(44) Cleij, T. J.; King, J. K.; Jenneskens, L. W. *Macromolecules* **2000**, *33*, 89–96.
(45) Yamamoto, M.; Kashiwagi, Y.; Nakamoto, M. *Langmuir* **2006**, *22*, 8581–8586.
(46) Shon, Y. S.; Cutler, E. *Langmuir* **2004**, *20*, 6626–6630.
(47) Taleb, A.; Petit, C.; Pileni, M. P. *Chem. Mater.* **1997**, *9*, 950–959.
(48) Kim, Y. R.; Lee, M.; Thorne, J. R. G.; Hochstrasser, R. M. *Chem. Phys. Lett.* **1988**, *145*, 75–80.
(49) Cheng, D.; Xu, H. Q. *Chem. Commun.* **2007**, 248–250.
(50) Thomas, J. B.; Brian, L. G. *J. Am. Chem. Soc.* **1985**, *107*, 8297–8299.
(51) Trefonas, P., III; Djurovich, P. I.; Zhang, X. -H.; West, R.; Miller, R. D.; Hofer, D. *J. Polym. Sci., Polym. Lett. Ed.* **1983**, *21*, 819.